CISM International Centre for Mechanical Sciences 598
Courses and Lectures

Teodor Burghelea
Volfango Bertola *Editors*

Transport Phenomena in Complex Fluids

International Centre for Mechanical Sciences

Springer

CISM International Centre for Mechanical Sciences

Courses and Lectures

Volume 598

For more than 40 years the book series edited by CISM, “International Centre for Mechanical Sciences: Courses and Lectures”, has presented groundbreaking developments in mechanics and computational engineering methods. It covers such fields as solid and fluid mechanics, mechanics of materials, micro- and nanomechanics, biomechanics, and mechatronics. The papers are written by international authorities in the field. The books are at graduate level but may include some introductory material.

More information about this series at http://www.springer.com/series/76

Teodor Burghelea · Volfango Bertola
Editors

Transport Phenomena in Complex Fluids

Springer

Editors
Teodor Burghelea
Laboratoire de Thermique
et Energie de Nantes
University of Nantes
Nantes, France

Volfango Bertola
School of Engineering
University of Liverpool
Liverpool, UK

ISSN 0254-1971 ISSN 2309-3706 (electronic)
CISM International Centre for Mechanical Sciences
ISBN 978-3-030-35557-9 ISBN 978-3-030-35558-6 (eBook)
https://doi.org/10.1007/978-3-030-35558-6

This Springer imprint is published by the registered company Springer Nature Switzerland AG
The registered company address is: Gewerbestrasse 11, 6330 Cham, Switzerland

Preface

Complex fluids refer to a broad class of liquids and soft materials with complex microstructure, which is characterised by length and timescales spanning over very large ranges. Examples include polymer solutions and melts, particle suspensions, colloidal gels, foams and emulsions. Unlike simple liquids, such as water, complex fluids exhibit a strongly nonlinear response to external forcing, which can be described by constitutive models where the stress tensor is a nonlinear function of the deformation rate tensor. This has dramatic consequences on the dynamics of complex fluids, at both microscopic and macroscopic levels, and on their ability to transfer or exchange mass, momentum and energy.

The practical importance of complex fluids is rapidly growing in industrial, pharmaceutical and life sciences applications as well as in everyday life. Whether we spread mayonnaise on a sandwich, rinse off the shower gel, blow our nose or sip a thick hot chocolate, we deal with complex fluids on a daily basis. Viscoplastic or viscoelastic gels and dense particle suspensions constitute most foods and pharmaceutical preparations, from pizza dough to painkiller tablets. Moreover, with a better understanding of liquid microstructures, industries have realised that working fluids can be tailored specifically to optimise existing processes, by altering their formulation (e.g. by means of chemical additives) in such a way as to change their dynamic behaviour and/or their properties.

This volume is based on the lectures delivered during the CISM Advanced Course 'Transport Phenomena in Complex Fluids' (Udine, Italy, 7–11 May 2018), which provide a thorough (although not exhaustive) overview of the topic, based on the most recent research results and the most updated methods for their analytical prediction and numerical simulation. The first chapter introduces the fundamental transport equations and gives and the main features of the most common constituents of complex fluids (polymers, surfactants and colloids), while the second chapter reviews the main nonlinear constitutive models; Chap. 3 presents an overview of the experimental methods to characterise the rheological and the interfacial behaviour. Chapters 4 and 5 provide an extensive description of transport phenomena in viscoelastic and viscoplastic fluids, respectively, with focus on the transport of momentum and energy. In Chap. 6, the dynamics of colloidal particles

suspended in a liquid medium is reviewed, while Chap. 7 provides an overview of the phenomenology of complex fluids with free surfaces. Finally, Chap. 8 introduces advanced, mesh-free numerical methods particularly suitable to model complex fluids from the macro- to the meso-scale.

The book is addressed to research scientists and professionals, engineers, R&D managers and graduate students in the fields of Engineering, Chemistry, Biology, Medicine, Applied and Fundamental Sciences, and can be used as support textbook in graduate and postgraduate courses in complex fluids or non-Newtonian fluid dynamics.

This book is dedicated to our lovely Mothers.

Liverpool, UK — Volfango Bertola
Nantes, France — Teodor Burghelea

Contents

Introduction to Transport Phenomena in Complex Fluids

Volfango Bertola

Abstract This chapter provides an overview of transport phenomena in fluids with complex microstructure. The first section reviews the general conservation equations, with focus on the issues arising when they are applied to complex fluids. The second section introduces different types of elementary constituents of complex fluids (polymers, surfactants and colloids).

1 Transport Phenomena

1.1 Advection and Diffusion

Simple transport processes (transport of mass, momentum and thermal energy) are described by the following conservation equation:

$$\alpha \frac{\partial \phi}{\partial t} + \nabla \cdot \mathbf{J}_\phi = 0 \tag{1}$$

where α is a phenomenological coefficient, ϕ is the characteristic potential of the transport process under consideration and $\mathbf{J}_\phi$ is the corresponding flux density. In the case of transport by *advection*, i.e. passive entrainment by the carrying fluid, the flux density is expressed as follows:

$$\mathbf{J}_\phi = \phi \mathbf{u} \tag{2}$$

where $\mathbf{u}$ is the fluid velocity. In the case of transport by *diffusion*, i.e. transport at molecular level, Eq. (1) is usually completed by linear constitutive equations (Fick's law, Newton's law and Fourier's law, respectively), which define the phenomenological relationship between flux densities and the generalized forces expressed in

V. Bertola (✉)
School of Engineering, University of Liverpool, Liverpool, UK
e-mail: Volfango.Bertola@liverpool.ac.uk

T. Burghelea and V. Bertola (eds.), *Transport Phenomena in Complex Fluids*,
CISM International Centre for Mechanical Sciences 598,
https://doi.org/10.1007/978-3-030-35558-6_1

the form of potential field gradients characteristic of each process, i.e. concentration gradient, velocity gradient and temperature gradient (Bird et al. 2007; Leal 2007):

$$\mathbf{J}_\phi = -\lambda \nabla \phi = \lambda \mathbf{F}_\phi \tag{3}$$

where λ is a phenomenological coefficient and $\mathbf{F}_\phi$ is the generalized force inducing the flow. The combination of Eqs. (1) and (3) leads to the well-known diffusion equation:

$$\alpha \frac{\partial \phi}{\partial t} = \frac{\lambda}{\alpha} \nabla^2 \phi \tag{4}$$

It can be shown that Eq. (4) can be expressed in Liouville's form (i.e. as a continuity equation), after introducing a suitable intrinsic velocity, $\mathbf{u}_\phi$, of the transport process under consideration (Bertola and Cafaro 2010):

$$\begin{aligned} &\frac{\partial \phi}{\partial t} + \nabla \cdot (\phi \mathbf{u}_\phi) = 0 \\ &\mathbf{u}_\phi = -\beta \nabla (\ln \phi) \end{aligned} \tag{5}$$

The introduction of this formalism provides a straightforward proof of the equivalence between the diffusion equation and other well-known equations of mathematical physics, such as the Burgers equation and the Kardar–Parisi–Zhang equation (Bertola and Cafaro 2007).

Linear constitutive equations are particular cases of more general phenomenological relationships between flux densities and forces:

$$\mathbf{J}_\phi = \lambda |\mathbf{F}_\phi|^r \frac{\mathbf{F}_\phi}{|\mathbf{F}_\phi|} \tag{6}$$

Examples of nonlinear phenomenological relationships are the Ostwald–de Waele constitutive equation for non-Newtonian flows, and the constitutive equation derived from the Prandtl–Taylor analogy used in modelling turbulent flows (Bird et al. 2007; Leal 2007).

1.2 Generalized Conservation Equations (Multifield Approach)

Conservation equations state that the evolution in time of a given specific quantity, ρQ, is due to the contributions of its flux, $\mathbf{J}$, and of its generation (or destruction) rate, S, which correspond to a divergence term and to a source term, respectively. Thus, they can be written in compact form (Banerjee and Chan 1980) as follows:

Table 1 Meaning of the symbols Q, $\mathbf{J}$ and S used throughout Eqs. (7)–(14) $\mathbf{u}$ is the velocity, $\mathbf{I}$ is the Kronecker tensor, p is pressure, $\boldsymbol{\Sigma}$ is the stress tensor, $\mathbf{F}$ is the body force, e_i is the internal energy and q is the heat flux. By replacing Q, $\mathbf{J}$ and S with the appropriate quantities, one obtains the different conservation equations (either local and instantaneous or averaged)

Quantity	Q	$\mathbf{J}$	S
Mass	1	0	0
Momentum	$\mathbf{u}$	$p\mathbf{I} - \boldsymbol{\Sigma}$	$\mathbf{F}$
Energy	e_i	$q + \mathbf{u} \cdot (p\mathbf{I} - \boldsymbol{\Sigma})$	$\mathbf{F} \cdot \mathbf{u}$

$$\frac{\partial \rho Q}{\partial t} + \nabla \cdot (\rho \mathbf{u} Q) = -\nabla \cdot \mathbf{J} + \rho S \tag{7}$$

where ρ is density, $\mathbf{u}$ is the fluid velocity and the values for Q, $\mathbf{J}$ and S are given in Table 1.

These equations hold inside each domain V_k, so that one obtains a set of conservation equations in differential form:

$$\frac{\partial \rho_k Q_k}{\partial t} + \nabla \cdot (\rho_k \mathbf{u}_k Q_k) = -\nabla \cdot \mathbf{J}_k + \rho_k S_k \tag{8}$$

In order to put the problem into a treatable form, the local conservation equations are averaged over the control volume and then ensemble averaged; the two operations can be inverted without changing the final result (Delhaye and Achard 1977). Here, averages are performed according to the following standard procedure (Banerjee and Chan 1980), where ensemble (spatial) averaging is denoted by angle brackets, and overbars indicate time-averaged quantities:

$$\frac{1}{V} \int_{V_k} \left\{ \frac{\partial \rho_k Q_k}{\partial t} + \nabla \cdot (\rho_k \mathbf{u}_k Q_k) \right\} dV = \frac{1}{V} \int_{V_k} \{ -\nabla \cdot \mathbf{J}_k + \rho_k S_k \} dV \tag{9}$$

Using the Leibniz rule[1] and to the Gauss theorem,[2] one obtains

[1] Leibniz rule:

$$\frac{\partial}{\partial t} \int_{V(\mathbf{x},t)} F dV = \int_{V(\mathbf{x},t)} \frac{\partial F}{\partial t} dV + \int_{\partial V(\mathbf{x},t)} F(\mathbf{u} \cdot \mathbf{n}) dA$$

It is analogous to the Reynolds transport theorem.

[2] Gauss theorem:

$$\int_{V(\mathbf{x},t)} (\nabla \cdot \mathbf{F}) dV = \nabla \cdot \int_{V(\mathbf{x},t)} \mathbf{F} dV + \int_{\partial V(\mathbf{x},t)} (\mathbf{F} \cdot \mathbf{n}) dA$$

If V does not depend explicitly on $\mathbf{x}$, the first term on the r.h.s. vanishes.

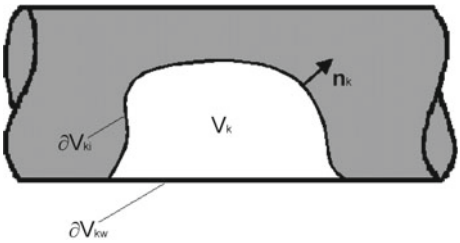

Fig. 1 Example of two-field modelling and notation used throughout this section

$$\frac{\partial \epsilon_{k,3} \langle \rho_k Q_k \rangle_{V_k}}{\partial t} + \nabla \cdot \epsilon_{k,3} \langle \rho_k \mathbf{u}_k Q_k \rangle_{V_k} = \epsilon_{k,3} \langle \rho_k S_k \rangle_{V_k} + \\ - \frac{1}{V} \int_{\partial V_{ki}} \mathbf{n}_k \cdot [(\mathbf{u}_k - \mathbf{u}_i)\rho_k Q_k + \mathbf{J}_k] dA - \frac{1}{V} \int_{\partial V_{kw}} (\mathbf{n}_k \cdot \mathbf{J}_k) dA \tag{10}$$

where $\epsilon_{k,3}$ is the volume fraction occupied by the k-th domain, $\mathbf{n}_k$ is the outward unit vector normal to the domain boundary, ∂V_{ki} is the part of the domain boundary in contact with other domains (interfacial boundary), ∂V_{kw} is the part of the domain boundary in contact with the wall, $\mathbf{u}_k$ and $\mathbf{u}_i$ are the domain and the interface velocities, respectively; an example of averaging volume containing two domains is shown in Fig. 1. Finally, Eqs. (10) are ensemble averaged:

$$\overline{\frac{\partial \epsilon_{k,3} \langle \rho_k Q_k \rangle_{V_k}}{\partial t}} + \nabla \cdot \epsilon_{k,3} \langle \rho_k \mathbf{u}_k Q_k \rangle_{V_k} = \overline{\epsilon_{k,3} \langle \rho_k S_k \rangle_{V_k}} + \\ \overline{- \frac{1}{V} \int_{\partial V_{ki}} \mathbf{n}_k \cdot [(\mathbf{u}_k - \mathbf{u}_i)\rho_k Q_k + \mathbf{J}_k] dA - \frac{1}{V} \int_{\partial V_{kw}} (\mathbf{n}_k \cdot \mathbf{J}_k) dA} \tag{11}$$

Double averaging ensures the continuity of first derivatives, which otherwise might be discontinuous; this could happen, for instance, in certain regions where field interfaces move in a deterministic manner in time or are stationary, where ensemble averaging alone leads to discontinuities.

Interface conditions Across the domain boundary, it is necessary to impose the conservation of fluxes:

$$\sum_k \frac{1}{V} \int_{\partial V_{ki}} \mathbf{n}_k \cdot [(\mathbf{u}_k - \mathbf{u}_i)\rho_k Q_k + \mathbf{J}_k] dA = 0 \tag{12}$$

Since the calculation of fluxes at the interface is not easy, sometimes it is preferable to cancel this term by adding up together the conservation equations in adjacent domains, obtaining the so-called mixture models:

$$\sum_k \left\{ \frac{\partial}{\partial t} \left(\overline{\epsilon_{k,3} \langle \rho_k Q_k \rangle_{V_k}} \right) + \nabla \cdot \overline{\epsilon_{k,3} \langle \rho_k \mathbf{u}_k Q_k \rangle_{V_k}} + \nabla \cdot \overline{\epsilon_{k,3} \langle \mathbf{J}_k \rangle_{V_k}} \right\} =$$

$$= \sum_k \left\{ \overline{\epsilon_{k,3} \langle \rho_k S_k \rangle_{V_k}} - \overline{\frac{1}{V} \int_{\partial V_{kw}} (\mathbf{n}_k \cdot \mathbf{J}_k) dA} \right\} \tag{13}$$

Although Eqs. (13) look simpler than Eqs. (11), all the information regarding the interfaces have been lost. On the other hand, the interface behaviour is essential in describing such phenomena as phase transitions or chemical reactions; thus, it is necessary to reintroduce into the model the lost information, by means of the so-called closure relationships.

Closure relationships The averaged conservation equations alone cannot be solved, even with the appropriate interface and boundary conditions, because their number is smaller than the number of unknowns. This happens because while double averaging the conservation equations allows reducing two-phase flow modelling to a mathematically treatable problem, at the same time it erases the local and instantaneous details, which must be reintroduced into the model by means of the so-called closure relationships or constitutive equations. These relationships provide additional equations in a sufficient number to equal the number of unknowns in order to 'close' the problem; they include equations of state, stress–deformation relationships, etc., and are often empirical or semi-empirical. Most closure relationships are flow-regime dependent, so that the overall accuracy decreases if they are applied to different flow patterns. A discussion on the different ways to solve the closure problem is presented, for instance, in Yadigaroglu and Lahey (1976). Closure relationships are usually sorted into two categories: interface closures, if they relate quantities across the domain boundary, and internal closures, if they relate quantities inside a domain.

Interface closures involve mass, momentum and energy fluxes at the interfaces between contiguous domains and between the domains and the pipe walls (the mass flux and the energy flux vanish for impermeable and adiabatic walls, respectively). For example, in case of evaporation or condensation, the mass flux at the interface is related to the heat flux by the phase transition heat, Δh_{LG}:

$$\left| \frac{1}{V} \int_{\partial V_{ki}} \rho_k \mathbf{n}_k \cdot (\mathbf{u}_k - \mathbf{u}_i) dA \right| = \frac{1}{\Delta h_{LG}} \left| \frac{1}{V} \int_{\partial V_{ki}} \rho_k (\mathbf{n}_k \cdot \mathbf{q}_k) dA \right| \tag{14}$$

The main problems in developing interface closures arise due to the fact that the interface geometry is generally very complex. As to wall conditions, the problem often reduces to the calculation of shear stresses, for which single-phase flow correlations are used.

Besides interface closures, more equations can be specified inside the domain, such as the equations of state. In particular, relations expressing the average value of the product of fluctuating quantities are required: in fact, in Eq. (10), one can find terms like $\langle \rho_k \mathbf{u}_k \rangle$ and $\langle \rho_k \mathbf{u}_k \mathbf{u}_k \rangle$, which are analogous to Reynolds stresses in turbulent flows. In two-phase flow, these quantities are even more difficult to be described,

because their fluctuations with respect to the mean value depend both on the turbulence inside each domain, and on the distribution of the phases over the averaging volume: although there is a strong reciprocal interaction between turbulence and flow pattern, their length scales are very different, so that modelling Reynolds stress-like quantities is not trivial.

1.3 Complex Fluids Versus Simple Fluids

The solution of the transport equations outlined in Sects. 1.1 and 1.2 strongly depends on the fluid structure, modelled through appropriate constitutive equations, and, in particular, on the *characteristic length*, i.e. the typical size of the fluid elementary constituents, and on the *relaxation time*, which is the time necessary to return to thermodynamic equilibrium after the fluid has been perturbed.

In simple fluids (also called molecular fluids), the characteristic length is of the order of molecular length scales (10^{-10}–10^{-9} m), and the relaxation time is of the order of the timescale of thermal fluctuations ($\approx 10^{-15}$ s). Thus, simple fluids respond almost instantaneously to an external forcing, such as an applied stress or deformation. In complex fluids, both the characteristic length and the relaxation time can range over several orders of magnitude, depending on the size, shape and stiffness of their elementary constituents, and on the short- and long-range interactions arising among them. The qualitative chart displayed in Fig. 2 shows a comparison among fluids with different micro-structures based on these two fundamental parameters.

Whilst the behaviour of simple fluids is adequately described by linear phenomenological models, such as Fick's Law, Newton's Law and Fourier's Law, fluids with complex microstructure often require sophisticated phenomenological models that introduce strong nonlinearities in the conservation equations; in the case

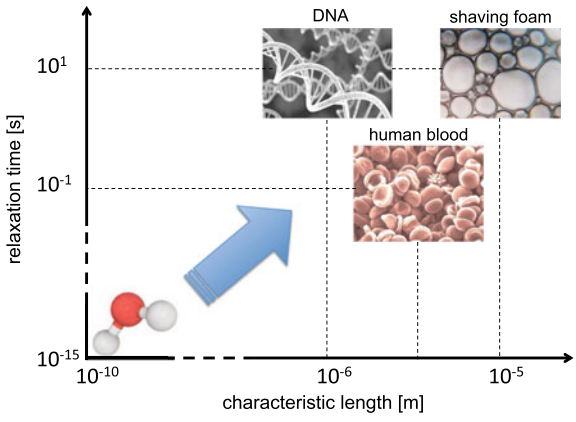

Fig. 2 Characteristic space- and timescales of complex fluids

of the equation of motion (momentum equation), these constitutive nonlinearities supplement the inertial nonlinearity characteristic of simple fluids at high Reynolds numbers.

2 Complex Fluids

2.1 Polymers

Polymers are high molecular weight molecules constituted by a large number of units, called monomers, connected by covalent bonds. A common example is polyethylene, $(C_2H_6)_n$, where the basic ethylene unit is repeated n times to form a long linear chain. Other common polymer structures are branched chains and chain networks.

Because of their structure, polymer molecules have a very large number of internal degrees of freedom, corresponding to rotations of C–C bonds[3]; thus, the same molecule can exhibit different instantaneous spatial arrangements, or *conformations*, which can be visualized schematically as a smoothed line segment. The longest sequence of monomers that behaves like a rigid rod defines the persistence length, L_p, which is a function of the backbone stiffness and electric charges distributed along the polymer chain. Thus, a simple way to describe linear chain polymers is to break down the chain into N segments represented by the position vectors of their end points, $\mathbf{a}_i$ $(i = 0...N)$, as shown in Fig. 3.

The end-to-end vector, $\mathbf{R} = \mathbf{a}_N - \mathbf{a}_0$, gives a measure of the actual molecule size; averaging over all molecules yields the root-mean-square end-to-end distance:

$$R_F = \sqrt{\langle \mathbf{R}^2 \rangle} = \sqrt{\langle (\mathbf{a}_N - \mathbf{a}_0)^2 \rangle} \tag{15}$$

A second quantity commonly used to measure the polymer molecule size is the *radius of gyration*, or the root-mean-square distance between the joints between consecutive vectors (Fig. 3) and the centre of mass. If the position of the centre of mass is indicated by vector $\mathbf{a}_G$, the radius of gyration can be calculated as follows:

$$R_g = \sqrt{\left\langle \frac{1}{N+1} \sum_{i=0}^{N} (\mathbf{a}_N - \mathbf{a}_G)^2 \right\rangle} = \sqrt{\frac{1}{N+1} \sum_{i=0}^{N} \langle (\mathbf{a}_N - \mathbf{a}_G)^2 \rangle} \tag{16}$$

In real polymer chains, two monomers cannot overlap, even partially, and occupy the same space; thus, a number of conformations that are ideally possible cannot be realized physically. This effect is known as the *excluded volume*, and has important consequences on the physics of polymer solutions (Strobl 1997; Teraoka 2002).

[3]Other internal degrees of freedom correspond to stretching of covalent bonds and oscillations of valence angles; however, their small amplitudes do not affect the molecule shape significantly.

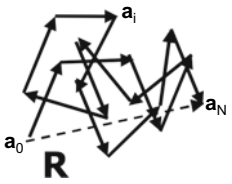

Fig. 3 Schematic representation of a linear polymer chain as a sequence of vectors

Because of excluded volume, real chains are bigger than ideal chains; in particular, for ideal chains $R_g \propto (N-1)^{1/2}$, while for real chains $R_g \propto (N-1)^{3/5}$ (Flory 1953).

The length of a polymer chain is, of course, proportional to its molecular weight. However, any polymer sample is a mixture of molecules with different degrees of polymerization, and monodisperse polymers (those with a single molecular weight) are exceptions. Polymers are usually polydisperse, and therefore their molecular weight is always the average value of a certain molecular weight distribution. If the polymer consists of n_i chains of exact molecular weight M_i, one can define a number-average molecular weight as

$$M_n = \frac{\sum_i n_i M_i}{\sum_i n_i} \tag{17}$$

and a weight-average molecular weight as

$$M_w = \frac{\sum_i n_i M_i^2}{\sum_i n_i M_i} \tag{18}$$

The ratio of Mw to Mn, called polydispersity index (PDI), is often used to express how polydisperse the polymer sample is

$$PDI = \frac{M_w}{M_n} = \frac{\sum_i n_i \sum_i n_i M_i^2}{\left(\sum_i n_i M_i\right)^2} \tag{19}$$

Many complex fluids are solutions of polymer molecules in a Newtonian solvent. While in the solid state, polymer molecules pack the space either in a regular array (crystalline phase) or at random (amorphous phase), in solutions each polymer molecule interacts with the surrounding solvent molecules, and may exhibit different conformations depending on the concentration.

For a given polymer, there are solvents that dissolve the polymer well (called *good solvents*), solvents that do not dissolve the polymer at all (called *nonsolvents*) and solvents with intermediate properties (called *poor solvents*) which can dissolve the polymer only up to a limited concentration. Tables of solvents and nonsolvents for different polymers can be found in the reference literature (Brandrup et al. 2005). In a good solvent, the solvent molecules impregnate the polymer coil, which swells increasing its volume; the solution remains clear and uniform even at concentrations

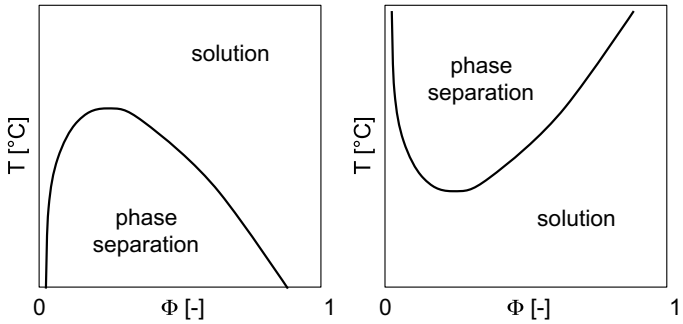

Fig. 4 Examples of phase diagrams of polymer solutions in temperature versus volume fraction coordinates. Left: phase diagram with upper critical temperature; right: phase diagram with lower critical temperature

as high as 100%. In a poor solvent, there is little affinity between the solvent molecules and the polymer coil, which, therefore, crumples reducing its volume. If a small amount of a nonsolvent is added to a polymer solution in a good solvent, the polymer precipitates as the nonsolvent mixes with the good solvent.

The quality of the solvent for a given polymer is strongly dependent on temperature. Thus, one can draw phase diagrams on the temperature versus volume fraction coordinate plane (Fig. 4) to identify the conditions to have a homogeneous solution and those to have phase separation. The qualitative phase diagrams of Fig. 4 indicate that at low volume fractions one has a stable solution over a large range of temperatures. For each polymer solution, there is a particular temperature, called the *theta temperature*, for which the solvent is poor just enough to compensate exactly the increase of the coil size due to the excluded volume effect. In this condition, the solution is called a *theta solution*, and polymer coils behave like ideal chains. For a rigorous thermodynamic analysis of the stability of polymer solutions, one can refer to Teraoka (2002).

A single polymer molecule interacting with the solvent takes a random coil conformation in order to maximize its conformational entropy, which is representative of the number of conformations with equivalent energy that is accessible to the polymer chain at a given temperature, and is defined as $S = k_B \ln(\omega)$, where k_B is Boltzmann's constant and ω is the total possible number of chain conformations. In the case of an ideal chain, one finds (de Gennes 1979)

$$S(\mathbf{R}) = S(0) - \frac{3R^2}{2\langle R^2 \rangle} \tag{20}$$

Equation (20) suggests that the more extended the chain, the lower its entropy, because an extended chain can adopt a fewer number of possible configurations as compared with the numerous possible equivalent conformations of a polymer coil. It can be shown that the variation of conformational entropy is equal to the

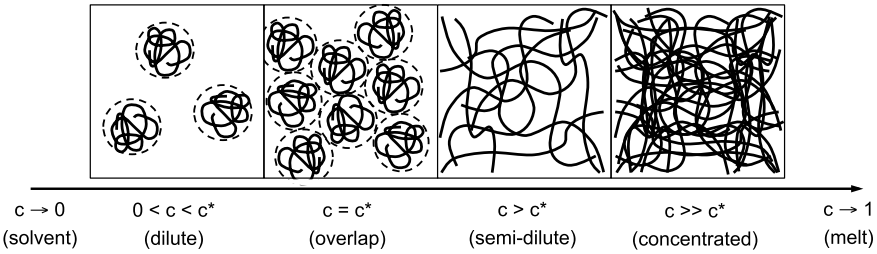

Fig. 5 Schematic illustration of the structure of polymer solutions as a function of the polymer concentration

conventional macroscopic entropy, $dS = \delta Q/T$, where δQ is the heat exchanged between the polymer chain and the environment, and T is temperature (Kittel and Kroemer 1980).[4]

If the polymer coil is stretched, for example, because of an applied stress or deformation, it reduces its conformational entropy, and therefore as soon as the constraint is removed, it will return to a maximum entropy conformation. This physical mechanism results into the viscoelastic behaviour of polymer solutions observed macroscopically, which is discussed in chapter "Transport Phenomena in Viscoelastic Fluids".

Figure 5 shows schematically the structure of polymer solutions as a function of the polymer concentration. At low concentrations, polymer coils are far from one another, i.e. the average distance between two polymer coils is much larger than their size, which defines the so-called *dilute solutions*. Thus, there are no interactions among polymer coils, which can be regarded as particles suspended in the fluid, and the solution viscosity can be estimated using Einstein's relationship for hard sphere suspensions:

$$\eta = \eta_s(1 + 2.5\Phi + ...) \tag{21}$$

where η_s is the viscosity of the pure solvent and Φ is the particle's volume fraction. One can also introduce a *specific viscosity*, or the ratio between the incremental viscosity and the solvent viscosity:

$$\eta_{sp} = \frac{\eta - \eta_s}{\eta_s} \tag{22}$$

and an *intrinsic viscosity*, defined as

$$[\eta]_0 = \lim_{c \to 0} \frac{\eta - \eta_s}{c\eta_s} \tag{23}$$

[4]One can verify empirically the equivalence of conformational entropy and macroscopic entropy by stretching an elastic rubber band. If the stretched rubber band is placed above the upper lip, where skin is most sensitive, and the pulling force is released, one feels cold: the stretched polymers return to a coiled conformation, and therefore increase their entropy, absorbing heat.

where c is the polymer mass concentration. The intrinsic viscosity is often calculated using the Mark–Houwink correlation:

$$[\eta]_0 = A \times M^b \tag{24}$$

where M is the molecular weight of the polymer, and A and b are empirical constants.[5]

As the polymer concentration is increased, the average distance between two coils progressively reduces until, at a critical concentration value c^* (the *overlap concentration*), it becomes approximately equal to the average size of coils, and the whole volume of the solution is packed with polymer coils. The overlap concentration can be calculated as follows:

$$c^* = \frac{1}{[\eta]_0} \tag{25}$$

Above the overlap concentration, interactions among polymer coils cannot be neglected, especially for those monomers located on the outer surface of the coil. In particular, electrostatic or hydrogen bonds between monomers belonging to the same macromolecule might break to form new bonds between monomers belonging to different chains. As a result, polymer coils unfold, and the solution structure appears as a network of overlapped and entangled polymer chains, characteristic of *semi-dilute solutions*, as illustrated schematically in Fig. 5. The change in the solution structure corresponds to a significant increase of viscosity, because the chain mobility is greatly reduced compared with the chains in dilute solutions; while in dilute solutions $\eta \propto c$, in semi-dilute solutions $\eta \propto c^2$.

At a higher concentration c^{**}, the solution enters the so-called *concentrated regime* in which each segment of the polymer chain does not have a sufficient space available. Typically, the volume fraction of the polymer at c** is between 0.2 and 0.3.

2.2 Surface-Active Agents (Surfactants)

Surfactants are molecules composed of a hydrophilic head group and a hydrophobic tail group. In other words, this means one side of the surfactant molecule has an affinity for the continuous phase (lyophilic), and the other side is incompatible with the continuous phase (lyophobic); overall, the surfactant molecule is amphiphilic (or amphipathic), i.e. it shows an affinity for different fluids at both ends.

The chemical structures suitable to act as either lyophilic or lyophobic sides of a surfactant molecule vary with the nature of the continuous phase (the solvent). If the solvent is a polar liquid such as water, which represents the most common case in practical applications, the lyophilic (hydrophilic) head is highly polar or ionic, while the lyophobic (hydrophobic) tail can be a hydrocarbon, fluorocarbon,

[5]For example, for polyethylene oxide $A = 0.0125$ and $b = 0.78$ (Brandrup et al. 2005).

perfluorocarbon or siloxane chain (Rosen 1978). In particular, the hydrophilic head can have different nature:

- *Cationic*, if the hydrophilic head has a positive charge;
- *Anionic*, if the hydrophilic head has a negative charge;
- *Non-ionic*, if the hydrophilic head has no apparent ionic charge;
- *Zwitterionic*, if the hydrophilic head has both positive and negative charges;
- *Amphoteric*, if the hydrophilic head can have either positive or negative charge depending on the pH of the solvent.

The hydrophobic tail can have a range of different structures; however, differences are less marked than in the case of the hydrophilic group. Usually, one can observe linear or branched hydrocarbon chains, or less frequently double chains or gemini structures where two surfactant molecules are joint in correspondence of their hydrophilic heads.

The relative strength of the hydrophilic and hydrophobic parts of a surfactant molecule is expressed by the hydrophilic to lipophilic balance (HLB), which can be calculated based on the molecular weight (Griffin 1949, 1954):

$$HLB = 20\frac{M_h}{M} \tag{26}$$

where M_h is the molecular weight of the hydrophilic head and M that of the whole surfactant molecule. An alternative approach to calculate the HLB number is to attribute different values to specific chemical groups in the molecule (Davies 1957). Low values of the HLB number indicate the hydrophobic tail outweighs the hydrophilic head, and vice versa high values indicate the surfactant behaviour is dominated by the hydrophilic part. Thus, the HLB number can be used to determine the solubility of a given surfactant in water, and the characteristics of oil–water emulsions containing it (see Table 2). Despite the use of the HLB number as a method to characterize surfactant systems has become common practice in academia as well as in the surfactant industry, one must keep in mind it leads to purely indicative conclusions, because it accounts only for the properties of the surfactant molecule rather than those of the whole system under consideration.

Table 2 Solubility in water and emulsion morphology obtained within different ranges of the HLB number

HLB number	Solubility in water	Emulsion morphology
1–4	Insoluble	Water in oil
4–7	Poor dispersion	Water in oil
7–9	Stable opaque dispersion	–
10–13	Hazy solution	Oil in water
>13	Clear solution	Oil in water

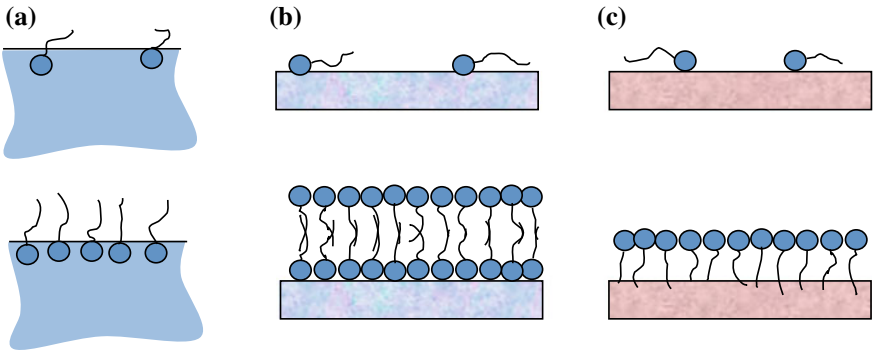

Fig. 6 Schematic picture of surfactant adsorption at fluid–fluid interfaces (**a**), on hydrophilic (**b**), and on hydrophobic surfaces (**c**), for low (top) and high (bottom) bulk concentrations

When surfactants are present in a fluid system at low concentration, they tend to adsorb onto free surfaces or interfaces between any two immiscible phases, oriented according to the affinities of their head and tail groups. When surfactants accumulate at an interface, they reduce its energy level, making it more thermodynamically stable. This makes surfactants essential components in several formulations, including inks, dyes, lubricants, gellants, paints and many others. Figure 6 displays examples of surfactant adsorption at fluid–fluid interfaces, hydrophilic surfaces and hydrophobic surfaces, at both low and high bulk concentrations. Remarkably, on hydrophilic surfaces, one can observe the formation of a double layer to ensure hydrophilic heads are exposed to the solvent.

A relation between the bulk surfactant concentration, C, and the surfactant adsorption, C^S, is provided by the Langmuir adsorption isotherm (Langmuir 1918):

$$C^S = C^S_\infty \frac{C}{C + a} \tag{27}$$

where C^S_∞ is the maximum possible adsorption at the surface when $C \to \infty$ and a is a constant which can be related to the energy of adsorption per molecule. Equation (27) can be generalized to account for the interaction between the adsorbed surfactant molecules and, in case of ionic surfactant, for the electrostatic energy of the surfactant ions (Borwankar and Wasan 1988). Other types of adsorption isotherms can be obtained based on various equations of state (Jho and Burke 1983; van Hunsel et al. 1986; Fainerman and Miller 1995). Figure 7 displays an example of adsorption isotherm as a function of the bulk concentration, together with sketches of typical surfactant distributions observed at different surfactant concentrations.

In general, surfactant adsorption occurs in two stages: (i) diffusion of surfactant from the bulk solution to the region near the interface and (ii) transfer of the surfactant molecules from this region to the interface. Thus, depending on the relative kinetics of the two stages, one can observe diffusion-controlled adsorption, where the surfactant

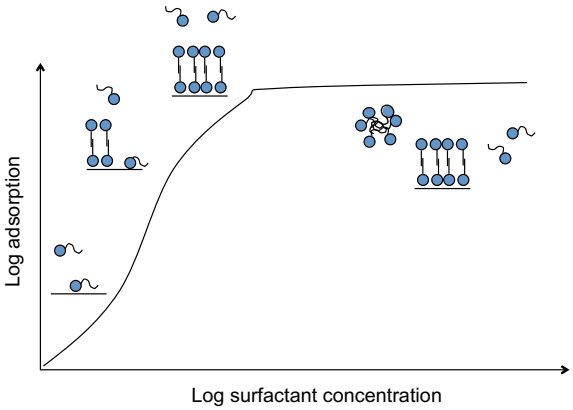

Fig. 7 Qualitative adsorption curve of a surfactant onto a hydrophilic surface as a function of the bulk concentration

diffusion is much slower than the second stage, and hence determines the rate of adsorption, and barrier-controlled adsorption, where the second stage is much slower than diffusion due to the presence of some kinetic barrier, which slows down the transfer of the surfactant molecules from the region near the interface to the adsorption monolayer. The adsorption kinetics may also be affected by electrostatic interactions in case of ionic surfactants and, if surfactant aggregates are present in the bulk, by reactions of aggregate formation and decay.

When the surface or interface is nearly at maximum coverage, molecules begin to aggregate in the bulk phase to minimize further free energy. This occurs at a well-defined concentration, specific to each surfactant-fluid system, known as the critical micellar concentration (CMC). Above the CMC, the system then consists of an adsorbed monomolecular layer at the interface, and of free monomers and surfactant aggregates (micelles) in the bulk, with all these three states in equilibrium (see the sketch in Fig. 7).

Typically, micelles are clusters of ∼50–∼200 surfactant molecules, whose size and shape are governed by geometric and energetic considerations (Israelachvili 2011). These self-assembled aggregates are structured in such a way so as to expose the lyophilic (hydrophilic) part to the solvent, and to conceal the lyophobic (hydrophobic) part inside, and therefore their shape is usually spherical or rod like, as shown in Fig. 8a. If micelles are highly packed, they may rearrange into ordered structures, generating hexagonal or lamellar phases (Fig. 8b).

The phase behaviour of a given surfactant system can be usefully portrayed in binary or ternary phase diagrams, such as the example shown in Fig. 9a, which displays the occurrence of different phases as a function of temperature and of the surfactant concentration, for a well-known surfactant system, sodium dodecyl sulphate–water (Kékicheff et al. 1989). Since surfactant phases can be strongly anisotropic, such as in the case of hexagonal or lamellar phases, they may affect significantly the behaviour of surfactant systems in shear flow; in particular, the transition from an isotropic phase (e.g. a dispersion of spherical micelles) to a lamellar phase (or vice versa) can change the apparent shear viscosity of the system of orders

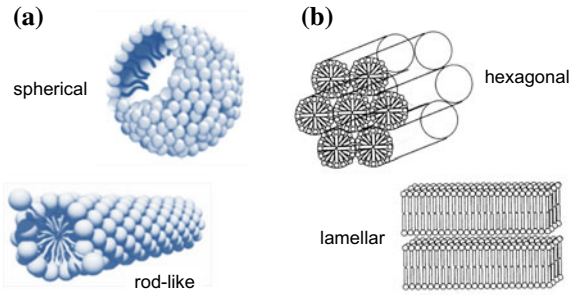

Fig. 8 Examples of surfactant aggregates or micelles (**a**), and examples of surfactant phases (**b**)

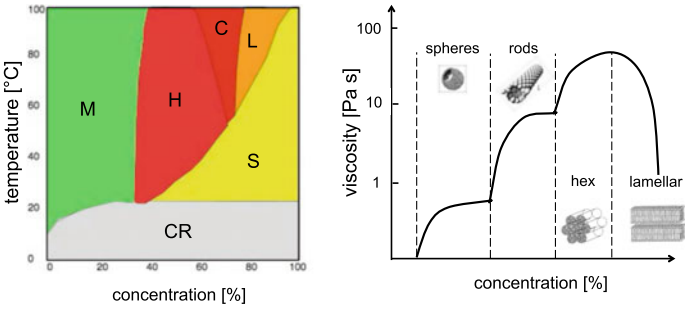

Fig. 9 Binary phase diagram of the sodium dodecyl sulphate–water system (Kékicheff et al. 1989) displaying: micelles, M; hexagonal phase, H; cubic phase, C; lamellar phase, L; phase separation, S; crystal phase, CR (**a**). Qualitative plot of shear viscosity as a function of surfactant concentration (**b**)

of magnitude, as shown in the example given in Fig. 9b, where viscosity drops in the transition from hexagonal packing to lamellar phase because in the latter the surfactant bilayers can shear on each other with the solvent acting as a lubricant.

The transition from isotropic to non-isotropic phases in surfactant systems may occur even without changing the structure of surfactant aggregates; sometimes, it is sufficient a change in the micelle conformation under shear flow. Shear-induced phase transitions are very common in liquid crystals and worm-like micellar solutions (Fischer and Callaghan 2001; Cates and Fielding 2006). For example, a surfactant system containing rod-like micelles with large aspect ratio will appear isotropic at zero or low shear rates; however, at high shear rates, micelles will align parallel to the flow direction, inducing a transition to a nematic phase.

Interfacial behaviour of surfactant solutions Interfaces between two immiscible fluids represent a boundary across which there is a more or less abrupt change of the fluid structure, and, in particular, of the intermolecular forces characteristic of the two phases. To compensate this difference, an interfacial tension arises in the interfacial region; in the case of interfaces between a liquid and a gas, where intermolecular interactions are negligible, this is called the *surface tension*. Although fluid interfaces

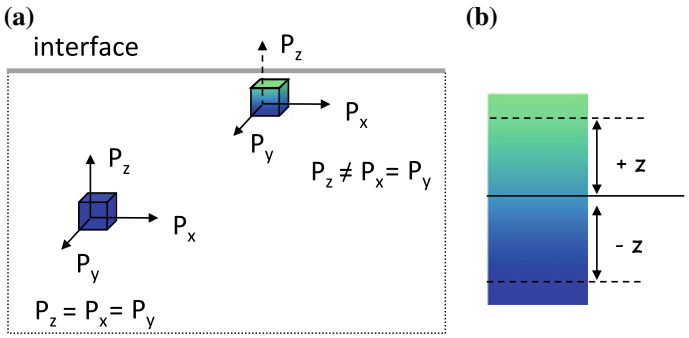

Fig. 10 Schematic description of pressure anisotropy on a fluid element near the surface as opposed to one in the bulk fluid (**a**), and normal cross section of a real fluid interface displaying the mutual diffusion layer (**b**)

are usually represented as mathematical surfaces with no thickness, in reality, they can be identified with a layer of small but finite thickness where the two fluids mix due to Brownian diffusion.

From the point of view of classical mechanics, surface tension is understood as a pressure anisotropy. With reference to Fig. 10a, pressure is isotropic in the bulk fluid, i.e. $p_x = p_y = p_z$; however, the presence of the surface creates a local anisotropy, and therefore near the surface $p_x = p_y \neq p_z$. Integrating the difference between the tangential and normal pressure components over the interface thickness, $2z$ (i.e. the thickness of the mutual diffusion layer, see Fig. 10b), yields the surface tension:

$$\gamma = \int_{-z}^{+z} |p_n - p_t| \, d\xi \tag{28}$$

where $p_t = p_x = p_y$ and $p_n = p_z$. Equation (28) shows its dimensions are force per unit length.

From the point of view of thermodynamics, surface tension represents a Gibbs excess property of the interface, namely, the energy per unit area of the interface. Since energy is an extensive quantity, the surface energy is proportional to the surface area; the larger the area, the larger the number of molecules that must be extracted from the bulk to create the new surface, which requires more work against the intermolecular forces. If increasing the surface requires work, then in the plane tangent to the surface there is a force opposing the expansion and perpendicular to the surface boundary, as shown schematically in Fig. 11a. For a homogeneous surface, the force per unit length is constant, and if a boundary of length L moves over a distance dx in the direction of the force, the work required to increase the surface area is

$$dW = \gamma L dx = \gamma dA \tag{29}$$

The Gibbs free energy of the surface then writes (Gibbs 1961):

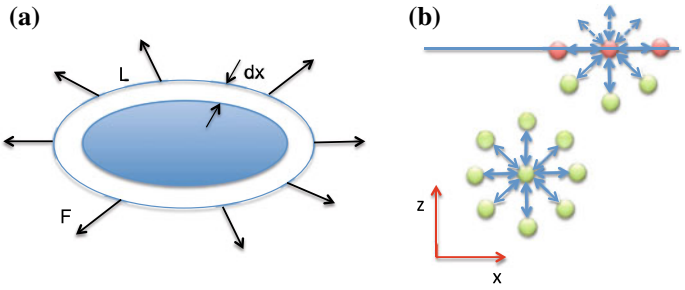

Fig. 11 Work of forces acting on the boundary of a fluid interface (**a**), and schematic description of molecular interactions in the bulk fluid and at the interface (**b**)

$$dG = -SdT + pdV + \gamma dA \tag{30}$$

and for a transformation at constant pressure and temperature, surface tension can be defined as

$$\gamma = \left(\frac{dG}{dA}\right)_{T,P} \tag{31}$$

Similarly, the surface tension can be defined in terms of the Helmholtz free energy for a process at constant temperature and volume. A remarkable feature of the thermodynamic approach is that the Gibbs interface is a mathematical surface with no thickness, whereas real surfaces extend over the mutual diffusion layer.

Finally, from the point of view of statistical mechanics surface tension arises from the imbalance of intermolecular forces at an interface, which is represented schematically in Fig. 11b. Thus, surface tension can be computed directly, in principle at least, by adding up all the mutual interactions between molecule pairs, by assuming, for example, a Lennard-Jones interparticle potential. In any case, all statistical mechanics approaches to calculate surface tension take as starting point either Eq. (28), i.e. the classical mechanics definition (Kirkwood and Buff 1949), or Eq. (31), i.e. the thermodynamic definition (Triezenberg and Zwanzig 1972), and express pressure and free energy, respectively, as a function of the intermolecular potential and of the interfacial density profile and the direct correlation function (Hansen and Mc Donald 2013).

The surface tension of liquids decreases monotonically with increasing temperature, because intermolecular forces decrease with an increase of molecular thermal activity. Theoretically, the value of surface tension should become zero at the critical temperature, T_C, since at this temperature, the interface between a liquid and its vapour disappears, although for some liquids the interface disappears a few degrees below the critical temperature. According to the Eötvös correlation, the surface tension decreases with temperature as (Eötvös 1886)

$$\gamma = \frac{k}{V^{\frac{2}{3}}}\left(T_C - T\right) \tag{32}$$

where $k = 2.1 \times 10^{-7}$ J/(K·mol$^{2/3}$) is the Eötvös constant and the molar volume, V, is given by the ratio between the molar mass and density.

A direct consequence of interfacial tension is the existence of a pressure difference across any curved interface between two fluids, also known as Laplace pressure (Young 1805; Laplace 1805), which is proportional to the surface curvature according to the Young–Laplace equation:

$$\Delta p = \gamma = \left(\frac{1}{R_1} + \frac{1}{R_2} \right) = -\gamma \nabla \cdot \mathbf{n} \tag{33}$$

where R_1 and R_2 are the principal radii of curvature at a given point of the interface and $\mathbf{n}$ is the unit normal pointing out on the convex side of the interface in the same point. The Laplace pressure is responsible, for example, of the capillary rise of liquids in tubes of small diameter, and of the onset of nucleate boiling at temperatures higher than the saturation temperature of a liquid.

Interfacial tension also determines the orientation of interfaces in the vicinity of a three-phase contact line, which is of exceptional importance in the understanding of wetting phenomena. The balance of interfacial tensions at a solid–liquid–gas contact line yields the contact angle of a liquid drop deposited on a solid surface, θ, defined as the angle between the solid surface and the liquid-air interface on the side of the liquid phase (Young 1805):

$$\gamma_{SG} = \gamma_{SL} + \gamma_{LV} \cos\theta \tag{34}$$

where γ_{SG}, γ_{SL} and γ_{LV} are, respectively, the solid–gas, solid–liquid and liquid–gas interfacial tensions. Although Eq. (34) was originally understood as the balance of three surface tensions, it can be derived more rigorously by interpreting γ_{SG}, γ_{SL} and γ_{LV} as interfacial energies per unit area, and minimizing the total free energy of the system (Gibbs 1961).

When surfactants are adsorbed at fluid interfaces, they lower the value of the surface (or interfacial) tension, according to the Gibbs adsorption equation (Gibbs 1961; Ono and Kondo 1960; Adamson 1976):

$$d\gamma = -k_B T \sum_i C_i^S d \ln C_i \tag{35}$$

where k_B is the Boltzmann constant, T is temperature, C_i and C_i^S are, respectively, the bulk concentration and the surface concentration (adsorption) of the i-th component in the solution; the summation in Eq. (35) is carried out over all components. Integrating Eq. (35), and recalling Eq. (27), yields the Frumkin equation (Frumkin 1925), which relates the interfacial tension of a surfactant solution to the surfactant adsorption:

$$\gamma = \gamma_0 + k_B T \ln \left(1 - \frac{C^S}{C_\infty^S} \right) \tag{36}$$